2023-08-16

MicroRNA-210 regulates dendritic morphology and behavioural flexibility in mice

Watts, Michelle; Williams, Gabrielle; Lu, Jing; Nithianantharajah, Jess; Claudianos, Charles

Springer

http://doi.org/10.1007/s12035-020-02197-6

http://hdl.handle.net/10616/48754

MicroRNA-210 Regulates Dendritic Morphology and Behavioral Flexibility in Mice

Michelle Watts[1], Gabrielle Williams[2], Jing Lu[3], Jess Nithianantharajah[4,5]*, Charles Claudianos[6,7]*

[1]Queensland Brain Institute, The University of Queensland, Brisbane, QLD, 4072, Australia. michelle.watts@ki.se

[2]School of Psychological Sciences, Monash University, Melbourne, VIC, 3800, Australia. gabbywilliams@gmail.com

[3]School of Psychological Sciences, Monash University, Melbourne, VIC, 3800, Australia. jing.lu2@monash.edu

[4]The Florey Institute of Neuroscience & Mental Health, Melbourne, VIC, 3052, Australia.

[5]Florey Department of Neuroscience, University of Melbourne, Melbourne, VIC, 3010, Australia. jess.n@florey.edu.au

[6]Queensland Brain Institute, The University of Queensland, Brisbane, QLD, 4072, Australia.

[7]Centre for Mental Health Research, The Australian National University, Canberra, ACT, 0200, Australia. charles.claudianos@anu.edu.au

*These authors contributed equally.

Correspondence should be addressed to:

J.N. (jess.n@florey.edu.au) or C.C. (charles.claudianos@anu.edu.au)

ABSTRACT

MicroRNAs are known to be critical regulators of neuronal plasticity. The highly-conserved, hypoxia-regulated microRNA-210 (miR-210) has been shown to be associated with long term memory in invertebrates and dysregulated in neurodevelopmental and neurodegenerative disease models. However, the role of miR-210 in mammalian neuronal function and cognitive behavior remains unexplored. Here we generated Nestin-cre driven miR-210 neuronal knockout mice to characterise miR-210 regulation and function using *in vitro* and *in vivo* methods. We identified miR-210 localisation throughout neuronal somas and dendritic processes and increased levels of mature miR-210 in response to neural activity *in vitro*. Loss of miR-210 in neurons resulted in higher oxidative phosphorylation and ROS production following hypoxia and increased dendritic arbour density in hippocampal cultures. Additionally, miR-210 knockout mice displayed altered behavioral flexibility in rodent touchscreen tests, particularly during early reversal learning suggesting processes underlying updating of information and feedback were impacted. Our findings support a conserved, activity-dependent role for miR-210 in neuroplasticity and cognitive function.

KEYWORDS

microRNA, miR-210, neuronal plasticity, dendritic branching, behavioral flexibility, hypoxia.

INTRODUCTION

MicroRNAs (miRNAs) represent an important class of small regulatory RNAs enriched within the nervous system that function in post-transcriptional regulation of gene expression [1]. They have direct effects on messenger RNA (mRNA) stability and abundance, and are capable of regulating numerous target mRNAs through translational repression and mRNA decay in association with the RNA induced silencing complex (RISC) [2,3]. In recent years, increasing evidence has established miRNAs as critical regulators of neuronal development and synaptic plasticity, with new roles for neuronal miRNAs continually emerging [4–6]. Being subject to regulatory control at stages of transcription, biogenesis and turnover, miRNAs are highly configurable to spatial and temporal translational regulation which is necessary for modulating plasticity at discrete synapses. Localised, activity-dependent mechanisms of miRNA turnover are also known to occur in mammalian synapses involving miRNA transport in RNA granules, miRNA processing and degradation of miRNA:RISC complexes [7–9].

miRNA-210 (miR-210) is considered a master hypoxia-inducible miRNA (hypoxamiR) being consistently upregulated by hypoxic conditions. miR-210 is associated with regulating various physiological processes in numerous cell types including angiogenesis, cellular metabolism, cell-cycle regulation, apoptosis and DNA repair [10–12]. Dysregulation of miR-210 is also frequently linked with cancer and myocardial infarction, having both oncogenic and tumour suppressor functions in different cancer types [13–16]. Hypoxia is a common feature of tumours that enhances tumour survival through stimulating angiogenesis, primarily through vascular endothelial growth factor (VEGF). Correspondingly, miR-210 has been shown to promote VEGF-directed endothelial cell migration and capillary-like formation through ephrin-A3 *in vitro,* and increase epithelial cell proliferation and angiogenesis *in vivo* [17,18]. In mouse models, miR-210 has been found to rescue cardiac function following myocardial infarction by inhibiting apoptosis and increasing focal angiogenesis [19]. Consistent with its role in hypoxia and correlation with cancer, miR-210 is involved in the metabolic shift to glycolysis during hypoxia by downregulating iron-sulphur cluster scaffolding proteins required for conversion of citrate to isocitrate [10,20].

There is growing evidence for miR-210's role within the central nervous system. A transcriptome study from our lab using olfactory conditioning in the honeybee previously identified a number of miRNAs upregulated following long-term memory formation [21]. Among these, miR-210 showed the highest induction following olfactory conditioning, and antisense knockdown of miR-210 impaired memory recall in this model. Additionally, upregulation of miR-210 has been associated with age-related behavioral changes in the honeybee, and miR-210 is cyclically expressed in clock neurons modulating circadian phase locomotor activity in Drosophila [22–24]. Analogous to its functions in non-neuronal cell types, miR-210 overexpression in the adult mouse sub-ventricular zone stimulates angiogenesis and neural progenitor cell proliferation [25]. Similarly, within the developing mouse brain, miR-210 was found to be expressed within the embryonic neocortex and regulate neural

progenitor proliferation through cell-cycle gene, CDK7 [26]. miR-210 is also associated with hypoxia-ischaemic (HI) brain injury, being upregulated in patient serum following acute cerebral infarction and modulating metabolic deficits in rat neonatal HI brain injury [20,27]. Of note, significant dysregulation of miR-210 has been associated with neurological disorders including Alzheimer's disease (AD) and rodent models of epilepsy. Significant downregulation of miR-210 has been found in AD post-mortem samples in various brain regions including medial frontal gyrus and hippocampus at both early and late stages of disease, as well as in cerebrospinal fluid and serum of patients with AD or those with mild cognitive impairment who are at risk of developing AD [28–30]. Rodent models of temporal-lobe epilepsy have also identified differential miR-210 expression, predominantly overexpression in hippocampal regions in both chronic and acute epilepsy stages at time points ranging from 3 hours to 4 months following seizure induction [31–33]. Another rodent study also highlighted that in rats subjected to 4 weeks of ischemia, modulation of the more divergent miR-210-5p guide strand affected synaptic density in the hippocampus and spatial memory performance in the Morris water maze [34].

To investigate the role of miR-210 in mammalian neuronal function and plasticity, we recently examined miR-210 targets within the human neuroblastoma derived SH-SY5Y cell line. Pull-down of miR-210 bound mRNA identified a significant enrichment of age-related neurodegenerative pathways including Alzheimer's, Huntington's and Parkinson's diseases [35]. Dual-luciferase validation confirmed that miR-210 directly regulates several genes involved in neuronal plasticity as well as oxidative metabolism genes linked to neurodegenerative diseases. Collectively, these data suggest an important role for miR-210 in modulating neural activation and plasticity within the brain. Here we use a mouse model with conditional knockout of the miR-210 stem-loop region in the nervous system to examine functional effects at the cellular level *in vitro* and cognitive behavioral effects *in vivo* to further characterise miR-210 in a more complex mammalian model.

RESULTS

miR-210 is expressed in neurons and upregulated by neural activity in vitro

Neuroplasticity relies on localised transcriptional changes, therefore, associated miRNA regulation would require synaptic/dendritic localisation of mature miRNA [7,8]. To gain insight into the neuronal role of miR-210 we first examined endogenous miR-210 localisation *in vitro*, in wild type C57BL/6J primary mouse hippocampal neurons using a Fluorescent In-Situ Hybridisation (FISH) approach. In neurons at 21 days *in vitro* (DIV-21) miR-210-3p was detected throughout the cell soma and processes including positive detection within MAP2 positive dendritic branches and spines (Fig. 1a-c). No specific staining was observed following hybridisation with a Scramble-miR negative control probe (Fig. 1d-f).

Evidence of miR-210 upregulation following olfactory conditioning and dysregulation in disease suggests neural activity may modulate miR-210 expression [21,28–33]. Previous studies however have primarily assessed samples of whole brain or brain regions with a mixed cell population. To more directly determine whether miR-210 is upregulated in neuronal cells in response to activity, we examined miR-210 expression *in vitro* in wild-type mouse hippocampal neurons following neuronal activation. Neurons were exposed to transient depolarisation with high potassium (K^+) to induce *in vitro* long-term potentiation (LTP) [36] and we found that mature miR-210 was significantly increased after 24 h (Fig. 1g). As a secondary method of neural activation we utilised glycine-mediated chem-LTP, as described previously [37]. Similar to K^+ activation, miR-210 was significantly increased 24 h after chem-LTP (Fig. 1h), suggesting miR-210 is induced by activity in cultured neurons via multiple mechanisms. As miR-210 is transcriptionally regulated through a promotor hypoxia-response element, to further understand how miR-210 might be induced by neural activity, expression of hypoxia-inducible transcription factors, *Hif-1α* and *Hif-2α,* were also quantified. Although induction of *Hif-α* under hypoxic conditions occurs primarily via protein stabilisation, *Hif-1α* induction can also be detected at the mRNA level and transcriptional up regulation of *Hif-1α* has been identified in the rodent brain following forms of long term consolidation including passive avoidance learning and environmental enrichment [38–40]. As LTP is associated with multiple transcriptional waves, with upregulation of transcription factors during earlier phases and upregulation of associated targets in later phases of LTP [39,41,42], *Hif-1α* and *Hif-2α* were quantified following K^+ activation *in vitro* at 20 min, 5 h, 12 h and 24 h time points (Fig. 1i). No significant induction of *Hif-2α* mRNA was observed at any time-point, however *Hif-1α* mRNA levels were significantly increased 12 h after neuronal activation, highlighting *Hif-1α* as a possible mechanism of miR-210 induction under these conditions.

In vivo knockout of miR-210

To further investigate the neuronal function of miR-210 both *in vitro* and *in vivo*, we crossed Nestin-Cre mice with mice carrying a floxed miR-210 transgene [43] to generate miR-210 neuronal knockout mice (miR-210 KO; Supplementary Fig. 1a). Although some studies have examined miR-210 expression in the mouse brain during embryonic development and disease states, there has been limited quantitative analysis of basal miR-210 expression within the normal adult mouse brain. We therefore characterised miR-210 expression across different brain regions in adult littermate control mice homozygous for the transgene and lacking Nestin-cre (tg CTRL). We found that basal miR-210 expression in tg CTRL mice was highest within the hippocampus (>17-fold higher, $p < 0.0001$) (Supplementary Fig. 1b) correlating with previous studies on hypoxia-ischaemic injury, temporal lobe epilepsy and AD which detected miR-210 dysregulation within the hippocampus. Comparison of miR-210 KO and tg CTRL mice also determined successful depletion of mature miR-210 in the hippocampus of miR-210 KO mice (>120-fold reduction, $p < 0.0001$, Supplementary Fig. 1c).

Neuronal knockout of miR-210 alters metabolism and dendritic arbour morphology in vitro

miR-210 dysregulation has been repeatedly associated with metabolic regulation in various cell types as well as in cortical rat neurons *in vitro* following oxygen-glucose deprivation [10,20,44]. We therefore wanted to examine metabolic changes following hypoxia in cultured hippocampal neurons from our miR-210 KO mice. Mitochondrial membrane potential ($\Delta\Psi m$) was measured as an indicator of oxidative phosphorylation using the fluorescent compound tetramethylrhodamine, ethyl ester (TMRE) which is sequestered by active mitochondria. From this we found that TMRE intensity was significantly higher in the soma of miR-210 KO neurons after 48 in 1% O_2 (Fig. 2a-c). As oxidative phosphorylation is tightly linked to reactive oxygen species (ROS) production and cellular oxidative stress, levels of cellular ROS were also detected using the ROS reactive 2',7'-Dichlorofluorescin diacetate (DCFDA) compound. Similarly, to TMRE, DCFDA intensity was also significantly increased in miR-210 KO neurons following hypoxia (Fig. 2d-f). This indicates that knockout of miR-210 increased neuronal oxidative phosphorylation and ROS production in response to low oxygen, consistent with previously observed effects of miR-210 on metabolic regulation and correlating with de-repression of metabolic miR-210 target genes [20,35].

At the cellular level, changes in dendritic arbour morphology can be representative of altered neuronal development or function impacting dendritic spine and synapse formation, connectivity and plasticity. In Drosophila, miR-210 upregulation has been found to affect axonal and dendritic arbour morphology in certain clock neurons *in vivo* and in the Drosophila neuronal cell line BG3-C2 *in vitro* [24]. To examine the impact of miR-210 knockout on the morphology of mouse hippocampal neurons, Sholl analysis was performed on cultured neurons from miR-210 KO and tg CTRL mice at DIV-12 using *Map2* as a dendritic marker (Fig. 3a-b). We found miR-210 knockout neurons displayed increases in various dendritic parameters including the total number of dendritic intersections (Fig. 3c-d), length of dendritic arbours (Fig. 3e) and dendritic branching (Fig. 3f).

Knockout of miR-210 Increases Behavioral Flexibility and Reduces Repetitive Responding in Reversal Learning

As miR-210 has been previously associated with behavioral changes in invertebrate models including changes in olfactory learning [21,22,24] we wanted to investigate more complex learning and memory in our vertebrate model. We therefore tested mice in the pairwise visual discrimination and reversal learning tasks using the rodent touchscreen operant system, a valuable behavioral tool for assessing different cognitive functions within the same testing environment [45–50]. As this genetic strain has not previously been characterized, we first measured exploratory and locomotor function in the open field and accelerating rotarod tests and confirmed that miR-210 neuronal knockout did not affect basic locomotor capacity (Supplementary Fig. 2). Mice were subsequently trained in appetitive operant conditioning using a series of pre-training stages (Fig. 4a) [46]. Both

miR-210 KO and tg CTRL mice completed the pre-training stages at the same rate and in the minimum number of sessions (Fig. 4b), indicating loss of neuronal miR-210 did not impact simple instrumental learning.

Mice were next tested in the pairwise visual discrimination task [46,51] where they learned to discriminate between a rewarded (CS+) and an unrewarded (CS-) visual stimuli (Fig. 4c-d) [52]. On 'first-presentation' trials, correct responses were rewarded but incorrect responses resulted in a 'correction trial', where the same trial was repeated until a correct response was made [46]. While performance accuracy can be measured using correct/incorrect responses, responding on correction trials provides a valuable measure of behavioral flexibility to adapt responses. We observed a consistent trend between miR-210 KO and tg CTRL groups in the primary learning measures for acquisition of visual discrimination, in that miR-210 KO mice tended to perform slightly *better* than tg CTRL mice by requiring fewer trials (Fig. 4e), making fewer errors (Fig. 4f) and completing fewer correction trials (Fig. 4g) to reach the discrimination learning criterion. To further examine this trend, we analysed visual discrimination performance at a session level for the first four sessions (when all mice are represented prior to some mice reaching the learning criterion and advancing; Supplementary Fig. 3). Analysis of performance accuracy, perseverative index, time to complete sessions and various response latencies (e.g. correct response, incorrect response, reward collection, trial initiation) showed no statistically significant differences between groups, but we noted a trend for miR-210 KO mice to be *faster* at initiating the commencement of trials in sessions 3-4 (Supplementary Fig. 3g-i).

After acquiring visual discrimination, mice were tested on reversal learning where the designated CS+ and CS- stimuli were now switched (Fig. 5a) requiring mice to inhibit responding to the previously rewarded stimulus (now CS-) and learn the new stimulus-reward association, thus allowing us to measure cognitive flexibility [45]. For the reversal learning measures analysed, we consistently observed a significant main effect of session ($p < 0.001$) as expected, confirming all animals improved their performance with increasing testing sessions. We observed no differences in the rate of reversal learning (% accuracy) across sessions between miR-210 KO and tg CTRL mice (Fig. 5b). However, miR-210 KO mice displayed *greater* behavioral flexibility with a significantly reduced perseverative index, a measure of repetitive responding to an incorrect response (effect of genotype [*g*] = $p < 0.05$; genotype x session interaction [*g* x *s*] = $p < 0.0001$), which was most evident during the initial reversal learning sessions following the stimuli-reward contingency change, when the demands to be flexible and thus the likelihood to perseverate is high (Fig. 5c). We also observed a similar, consistent pattern for various latency measures during reversal learning, with miR-210 KO mice taking *less* time to complete sessions (*g* = $p < 0.001$; *g* x *s* = $p < 0.0001$) (Fig. 5d) and initiate the commencement of trials (*g* = $p < 0.01$; *g* x *s* = $p < 0.0001$; Fig. 5e) regardless of whether the previous response was correct (*g* = $p < 0.05$; *g* x *s* = $p < 0.001$; Fig. 5f) or incorrect (*g* = $p < 0.05$; *g* x *s* = $p < 0.05$; Fig. 5g), supporting the more subtle phenotypic trends observed during visual

discrimination. Interestingly, we did not see statistically significant differences in other response latency measures (correct response latency, Fig. 5h; incorrect response latency (data not shown); reward collection latency, Fig. 5i) highlighting the observed changes in trial initiation latency were not simply due to overt changes in motivation or motor capacity. Collectively, these data suggest loss of miR-210 impacts behavioral flexibility and the drive to continue engaging in the task and commence new trials, especially when contingencies in the environment change and updating of information is required.

DISCUSSION

Deciphering the role of miRNA regulation in neuronal plasticity is critical for understanding the molecular processes driving behavior and cognition disrupted in neurological disorders. Here we have utilised *in vitro* and *in vivo* methods to further understand the role of hypoxia-regulated miR-210 in neuronal function (Fig. 6). Our work builds on previous evidence of miR-210 targeting and involvement in neuronal plasticity, including dysregulation in AD and epilepsy as well as modulation of long-term recall following miR-210 knockdown in the honeybee. We detected increased levels of mature miR-210 in response to neuronal activation *in vitro* supporting neuronal activity-dependent modulation of miR-210. Increased oxidative phosphorylation and ROS levels following hypoxia and altered dendritic arbour morphology in mouse hippocampal neurons lacking miR-210 show an important functional role of miR-210 in vertebrate neurons, consistent with miR-210 metabolic functions in non-neuronal cell types as well as findings in invertebrate neuron models. *In vivo,* knockout mice displayed significantly enhanced behavioral flexibility in the touchscreen reversal learning task, exhibiting reduced perseverative behavior and increased drive to initiate engagement in the task. These observed alterations in distinct aspects of behavior reveal miR-210 plays an important role in the complex cognitive processes that underlie vertebrate learning and memory.

We found neuronal activity increased miR-210 mRNA in an *in vitro* model, however additional studies would be required to determine the direct mechanisms regulating miR-210 induction in neurons. Aside from studies finding HIF-1α transcriptionally upregulated following long-term consolidation [39,40] neuronal knockout of HIF-1α in mice has also been shown to impair spatial memory while HIF stabilization leads to improves hippocampal memory [53,54]. This warrants further investigation into the role of HIF-1α in cognition and how it relates to either hypoxic stabilisation of HIF-1α protein and/or or transcriptional upregulation of HIF-1α mRNA. These observations however support a potential model whereby increased metabolic demands occurring innately during neural activity lead to reduced cellular oxygen and HIF pathway induction [55].

Observed changes in dendritic arbour density in hippocampal neurons also support an important role for miR-210 in neuronal function. Previously, miR-210 has been found to promote axon regeneration in peripheral mouse neurons through targeting ephrin-A3 (EFNA3) [56]. As EFNA3

signalling is known to regulate axon guidance as well as dendritic morphology [57,58] this may contribute to the altered dendritic morphology we observe in miR-210 KO neurons. Metabolic function may also act as a rate-limiting factor for plasticity changes in neuronal processes and high metabolic demand and altered metabolism could therefore indirectly modulate neuronal morphology.

Previously, three separate studies have identified a significant downregulation of miR-210 in AD patients at both late and early stages of AD as well as in sufferers of mild cognitive impairment [28–30]. Both deficits in oxidative phosphorylation and increased oxidative stress in the brain are hallmarks of neurodegeneration and metabolic dysfunction is known to occur early in disease progression, preceding cognitive decline [55,59,60]. Identification of increased oxidative phosphorylation and ROS in miR-210 KO hippocampal neurons is therefore of interest and potentially significant to AD pathology. Collectively, this suggests that miR-210 downregulation may not just be ancillary to disease but may also exacerbate oxidative stress and metabolic dysfunction in the AD brain. Given that vascular dysfunction and hypoperfusion are major features of the AD brain, downregulation of hypoxia-induced miR-210 seems counter-intuitive. Accumulation of HIF-1α, however, is attenuated with age in ischemic tissues and this appears to be further exacerbated in AD with HIF-1α levels significantly decreased in patients compared to age-matched controls [61–63]. Reduction of HIF-1α and its targets within the AD brain, despite hypoperfusion, suggests that hypoxic induction of HIF-1α is inhibited in AD. Increased oxidative stress in the AD brain may play a role in this occurrence as ROS are known to promote HIF-1α degradation [64]. Further research is evidently needed to elucidate the role of HIF-1α and its regulatory targets such as miR-210 in AD pathology and how it relates to hypoxia and ROS.

While hypoxia is known to cause deficits in learning and memory [65,66], these effects appear to be independent of HIF pathway induction and dependent on the severity of hypoxic exposure with mild hypoxic preconditioning conferring protection to later hypoxic exposures through HIF-1α [67,68]. The role of HIF in discrete cognitive functions likely also relates to differing sensitivities of neuronal subpopulations to hypoxia. Within the brain, pyramidal excitatory projection neurons are known to be most sensitive to hypoxia, while inhibitory interneurons are most resistant [70,71]. Of interest, HIF-1α is induced in inhibitory interneurons but not pyramidal neurons in response to hypoxia [72]. Interneurons are thought to primarily function in excitatory control of cognitive processing and are involved in control of sensory input and cognitive flexibility in reversal learning [73–76]. Understanding interneuron function is of interest to both neurodegenerative and neuropsychiatric disorders, in particular, schizophrenia where parvalbumin GABAergic interneurons are selectively damaged and deficits are observed in various cognitive processes requiring inhibitory control including reversal learning [77–80]. Aside from schizophrenia, interneuron circuitry is also linked to Parkinson's disease, AD and obsessive-compulsive disorder and targeted ablation of interneurons leads to development of compulsive behavior and hyperkinetic motor dysfunction in mice [81–84]. Both inactivity and loss of interneurons associated with reductions in inhibition are also linked to

epilepsy syndrome [85,86]. Based on the hypoxic-resistance and HIF-1α expression of inhibitory interneurons as well as their established cognitive role, the observed improvements in reversal learning in miR-210 KO mice may relate to a functional role of HIF-1α in inhibitory interneurons. Cognitive processes affected in miR-210 knockout mice also align with circuitry affected in epilepsy, where miR-210 is overexpressed. Taken together these data implicate a role for miR-210 in behavioral flexibility and mechanisms regulating feedback and updating of information. Although beyond the scope of this study, inducible or cell-type specific knockout systems could establish specific neurocircuitry or cell populations where miR-210 may function during cognition.

Characterising mechanisms regulating neural function in response to activity is crucial to understanding plasticity within the healthy brain. Further understanding of the HIF pathway and miR-210 in cognition may also be critical to elucidating the molecular basis of neurological disorders such as AD where this pathway is disrupted. This study provides the first characterisation of a neuronal miR-210 knockout mice and the first behavioral analysis of a microRNA knockout mouse model using the rodent touchscreen assays, which may be an important tool for dissecting and identifying specific functions of miRNAs in regulation of complex cognitive processes. Data presented here highlights induction of miR-210 in response to neuronal activation and functional consequences of miR-210 knockout in hippocampal neurons *in vitro*. Identification of discrete cognitive processes affected in miR-210 knockout mice also provides important insights into miR-210's endogenous functions and supports a conserved role for miR-210 in learning and memory in more complex mammalian models.

MATERIALS AND METHODS

Animals

Heterozygous mice containing a floxed miR-210 allele (Mir210^{tmMtm}; JAX, Bar Harbour, US) [43] were inbred to produce homozygous mice (miR-210$^{loxP/loxP}$) and crossed with Nestin-Cre mice (B6.Cg-Tg(Nes-cre)1Kln/J, a kind gift from Dr Jason Cain) to produce miR-210 KO mice (miR-210$^{-/-}$;Nestin-Cre; Supplementary Fig. 1a) at the Monash Animal Research Platform (MARP, Monash University, Clayton, Australia). The cohort of adult male mice used for the behavioral studies were bred at Monash University and shipped to The Florey Institute of Neuroscience and Mental Health where all behavioral studies were completed. Except where otherwise stated animals were housed in standard light conditions with access to water and food *ad libitum*. All experiments were conducted in accordance with the Australian Code of Practice for the Care and Use of Animals for Scientific Purposes, and approved by Monash University and/or The Florey Institute of Neuroscience and Menth Health Animal Ethics Committees.

Primary Hippocampal Neurons

Hippocampal neurons were isolated from embryonic day 18.5 (E18.5) mice where the day of plug was designated as E0.5. Hippocampi were dissected in ice-cold dissection media (1X HBSS -Ca^{2+}/-Mg^{2+}, 100 U/mL Pen-Strep, 1m M Sodium-pyruvate, 20 mM HEPES and 25 mM Glucose). Hippocampi were digested for 20 min at 37°C in dissection media with 20 U Papain and 1% DNase-I, with gentle perturbation every 5 min. Digestion solution was removed from tissue and hippocampi washed 2-3X in warm neuronal medium (Neurobasal Medium, 1X GlutaMAX, 100 U/mL Pen-Strep, 5% Fetal Bovine Serum [FBS, Gibco, Thermo Fisher] and 1X B-27). Neurons were dissociated in 1 mL of neuronal medium using 3 consecutively smaller fire-polished pipettes. Cells were spun at 200 g for 5 min before filtering through a 70 µm cell strainer and plating in neuronal medium on poly-D-lysine coated plates (0.1 mg/mL) or coverslips (0.5 mg/mL) at 5 x10^4 cells/well. Neuronal medium was replaced after attachment (~4-6 h after plating) and again the following day with FBS free neuronal medium. Neurons were maintained in serum-free medium at 37°C/5% CO_2, exchanging 50% of medium every 3 days.

In Situ-Hybridisation in Cultured Neurons

Neurons were fixed in 4% PFA/4% Sucrose in PBS for 10 mins at room temp and washed 3 x 5 mins with PBS. Fixed neurons were deproteinated in 20 µg/mL Proteinase K in PBS for 10 min, before 2X 5 min PBS washes. To remove residual PBS, coverslips were incubated 2X 10 min in fresh imidazole buffer (0.13 M 1-methylimidazole, 300nM NaCl, pH 8.0). Cells were fixed in l-ethyl-3-(3-dimethylaminopropyl) carbodiimide (EDC) in imidazole buffer for 1-2 h in a humidified chamber. Cells were washed 1X with 0.2% (w/v) glycine in PBS and 2X in PBS for 5 min each before incubation in fresh acetylation solution (0.1M triethanolamine, 0.5% (v/v) acetic anhydride) for 10 min and washing

2X 3 min in PBS on shaker. Cells were then incubated in hybridisation buffer (50% formamide, 5X SSC, 250 µg/mL yeast tRNA, 500 µg/mL salmon sperm DNA, 5X Denhardt's solution, 2% Blocking reagent, 0.5 % Tween, 9.2 mM citric acid) for 1 h at hybridisation temperature (58°C). DIG-conjugated LNA probes for miR-210-3p or Scramble-miR (Exiqon) were denatured at 75°C for 4 min, cooled on ice, diluted in hybridisation buffer to 10 nM and added to coverslips for 16 h at hybridisation temp in a humidified chamber. Following hybridisation, cells were washed 3X 10 min in 0.1X SSC at 4-8°C above hybridisation temp with agitation. Coverslips were then washed in 2X 5 min in SSC on shaker before incubating 20 min in 3% H_2O_2/PBS. Cells were then washed 3X 3 min in Buffer I (100 mM Tris-HCl, 150 mM NaCl, pH 7.5) on shaker before a 30 min incubation in Blocking Buffer (100 mM Tris-HCl, 150 mM NaCl, 0.5% Blocking reagent, 0.5% BSA, 0.1% Tween). DIG was detected by incubation with mouse αDIG primary antibody (1:500; Perkin Elmer) and neurons also immunostained with αMAP2 (1:5000; Abcam, ab5392) diluted in blocking buffer for 1-2 h. Cells were washed 3X 5 min in Buffer II (100 mM Tris-HCl, 150 mM NaCl, 0.1% Tween) and MAP2 primary antibody detected with secondary antibody, goat αChicken IgY AlexaFluor® 647 (1:400; Abcam; ab150171) in blocking buffer, in a dark, humidified chamber on shaker at low speed for 1 hr and cells washed again 3X 5 min in Buffer II. Tyramide Signal Amplification (TSA®) with Fluorescein (Perkin Elmer) was diluted 1:50 in provided amplification diluent and added to coverslips for 10 min in the dark. Sections were then washed 3X 5 min in Buffer II and mounted in fluorescent mounting medium with DAPI. All images were taken on an upright Zeiss Axio Imager M2 fitted with a Zeiss Axio Cam 506 mono camera using the Zen 2 pro software. Image contrast was enhanced uniformly for figure preparation.

Mitochondrial Membrane Potential and ROS Detection

For detection of mitochondrial membrane potential or ROS in primary hippocampal neurons at DIV-10, cells were stained with TMRE (tetramethyl rhodamine ethyl ester) or DCFDA (2',7'-Dichlorofluorescin diacetate), respectively. Cells were washed 3X in Tyrode's buffer (145 mM NaCl, 5 mM KCl, 10 mM glucose, 1.5 mM $CaCl_2$, 1 mM $MgCl_2$, 10 mM HEPES, pH 7.4) before staining in 150 nM TMRE or 10 µM DCFDA diluted in Tyrode's buffer for 30 min at 5% CO_2/37°C. Stain was removed and cells washed three times in Tyrode's buffer before imaging. Fluorescent and DIC images for each experiment were collected using the same gain and exposure settings and fluorescent intensity was analysed using the ImageJ software.

Neuronal Activation

For neuronal activation using high concentration potassium (K^+), HEPES Buffered Saline (HBS; 90 mM KCl, 25 mM HEPES, 33 mM D-Glucose, 2 mM CaCl2, 2 mM MgCl2, 100 µM picrotoxin) was applied to neurons at 21 days *in vitro* for 3 x 1 sec intervals. High K^+ HBS application was followed by 10 sec recovery in control HBS (NaCl and KCl adjusted to 119 mM and 5 mM, respectively) before

replacement with neuronal media. As a control condition, neurons were incubated in control HBS for 30 sec. For glycine-induced Chem-LTP, DIV-18 hippocampal cultures were incubated at room temp for 5 min in extracellular solution (ECS; 150 nM NaCl, 2 mM $CaCl_2$, 5 mM KCl_2, 10 mM HEPES, 30 mM Glucose, 1 µM strychinine, 20 µM bicuculline methiodide). Neurons were then incubated in ECS with 200 µM glycine for 3 min at room temp before replacing neuronal medium. As a control condition, neurons were incubated 3 min in ECS without glycine.

RNA Extraction, cDNA Synthesis and Quantitative Real-Time PCR

RNA was extracted using TRIzol reagent as per manufactures directions, keeping samples on ice and using 20 µg of glycogen as a carrier. For brain regions, whole brains were dissected in ice-cold PBS and collected regions were diced with a scalpel and placed on dry ice. Tissue was disrupted in TRIzol solution by passing 5X through a 23-gauge needle. TRIzol incubation and chloroform phase separation steps were repeated twice with incubation times increased to 30 and 15 mins, respectively. Samples were quantified using a NanoDrop Lite spectrophotometer and Qubit RNA high sensitivity assay. Synthesis of cDNA for protein-coding gene expression was performed using SuperScript III RT according to manufacturer directions using oligo-dT and qRT-PCR reactions were performed in triplicate on the Roche LightCycler480 system using the QuantiNova SYBR Green PCR Kit (QIAGEN) at a melting temp (Tm) of 60°C. For miR-210 detection, a stem-loop reverse transcription primer was designed using a previously described template and annealed in a thermo-cycler (95°C/5 min, ramp to 25°C/1°C min^{-1}) [87]. cDNA was synthesised using 0.1 µM primer, 0.25 µL of RT and 0.1 µL of RNaseOUT/reaction and reverse transcription performed using a low-temp cycling program (16°C/30 min, 42°C/30 min, 85°C/5 min, 4°C/hold) as described previously [88,89]. For qRT-PCR, forward miRNA-specific primer was designed to be complimentary to the first 16 bp of the mature miR-210 sequence with an additional 4 bp's added to the primer 5' end to a final Tm of ~60°C. Reverse primer was a universal primer specific for the stem-loop region of the RT primer [87]. Forward primer was used at a final concentration of 1.5 µM and universal stem-loop reverse primer at 0.7 µM. For protein-coding genes, Tbp and Hprt1 were used for normalisation, for miR-210, Rn5s (in vitro experiments) and Rnu6 (in vivo) were used for normalisation. Primer sequences are as listed in Supplementary Table S1.

Scholl Analysis

Neurons were fixed at DIV-21 as described for In Situ hybridization and blocked for 30 min in 3% BSA, 0.3% TX in PBS at room temperate before adding chicken anti-MAP2 primary antibody diluted in 3% BSA/0.3% TX/PBS and incubating overnight at 4°C in a humidified chamber. Primary antibody was removed and cells were washed 3 times with 0.3% TX/PBS for 5 min. Cells were then incubated with secondary antibody, goat anti-Chicken IgY AlexaFluor® 647 in a dark, humidified chamber on shaker at low speed for 2 h. Secondary antibody was washed off with 3 x 5 min washes in PBS/TX and coverslips were mounted onto glass slides using fluorescent mounting media with DAPI (DAKO).

For analysis of primary neuron dendritic morphology, the Fiji distribution of ImageJ and Sholl plugin was used. Single channel fluorescent images of MAP2 staining were used for analysis and images were 'cleaned' to remove neuronal processes of neighbouring cells to generate images of isolated neurons as required for Sholl tracing. 8-bit Images were analysed as described in the plugin manual with starting radius set to 10 μM and radius step size set at 5 μM. Ramification index of branching was calculated as the ratio of the maximal number of intersections to the number of primary branches extending from the neuronal soma and the enclosing radius correlates to the largest radius at which intersections were detected.

Exploratory and Locomotor Behavioral Testing

For the locomotor open field test, a white open field mouse chamber (Med Associates, St. Albans, VT, USA) of dimensions 27.3 (L) x 27.3 (W) x 20.3 (H) cm in-built with an automated infrared tracking array controlled using the Activity Monitor system and software (v6.02, Med Associates) was used. Mice were moved into the testing room under low lighting conditions and habituated for at least 10 min before testing. Mice were tested individually and placed in the centre of the field and movement automatically tracked for a period of 60 min. For the accelerating rotarod task, mice were first familiarized to the rotarod (Ugo Basile, Gemonio, VA, Italy) by giving them a training period of 1 min with the rod rotating at constant speed of 4 rpm. Mice were then tested across three trials (with rests between trials) where the speed gradually accelerated from 4 to 40 rpm over a period of 5 min for each trial. Time spent on the rotarod was recorded as the latency to fall from the rod.

Touchscreen cognitive testing for pairwise visual discrimination and reversal learning

Adult male mice (12-13 weeks of age) were acclimatised to reverse light dark housing (lights off 07:00, lights on 19:00) for a minimum of two weeks prior commencing food restriction to reach 85-90% of baseline free-feeding weight as that previously described [51]. Mice were tested 5-7 days/week in the dark phase (active cycle) using the mouse touchscreen operant system (Campden Instruments Ltd, UK) with Whisker and ABET II Touch software. Mice were first pre-trained through five stages to acquire operant conditioning as that previously described [51]. Following completion of pre-training, all mice commenced the pairwise visual discrimination task on the same session [51]. For each trial in the pairwise visual discrimination task, two stimuli where presented in the two response windows in a pseudo-randomized manner (Fig. 4c). The two visual stimuli used were the 'plane' and 'spider' stimuli, with one designated as CS+ (correct) and the other as CS- (incorrect; Fig. 4d), counterbalanced across mice in both genotypes to minimize effects of potential stimulus bias. Sessions ended after the completion of 30 'first-presentation' trials or a maximum of 60 min. On 'first-presentation' trials, correct responses were rewarded but incorrect responses resulted in a time-out and a 'correction trial', where the same trial was repeated until a correct response was made. Mice were individually moved onto reversal learning the next training day after reaching the visual discrimination learning criterion of ≥80% accuracy for two consecutive sessions. Reversal

learning task sessions were run as that described for visual discrimination except that the designated CS+ and CS- stimuli were now switched (Fig. 5a). In order to control for and ensure all mice completed the same number of trials, the first reversal learning session was split across two sub-sessions (15 trials per session) [46]. If mice did not complete 15 trials within the first sub-session, the number of trials possible for the second sub-session was altered to achieve a total of 30 trials across the sub-sessions. All mice were tested on reversal learning for a total of 10 complete (30 'first presentation' trial) sessions.

Statistics

Statistical analyses were carried out in GraphPad Prism v8.2.0. Significance was calculated at a 95% confidence interval ($\alpha = 0.05$). Homogeneity of variance and data normality distribution was determined using Levene and Shapiro-Wilk tests, respectively. For cell and molecular data, specific means tests and appropriate post hoc analyses were used as indicated in the text. For behavioural data, we performed two-sample t-tests or for session level analyses of visual discrimination and reversal learning, a two-way repeated measures ANOVA or a mixed-effects model with genotype as a between-subjects factor and session as a within-subjects factor, and post hoc Sidak's multiple comparisons analysis when there was a significant genotype x session interaction. Note, due to the nature of multiple comparisons testing, we observed instances of significant genotype x session interactions but no significant post hoc comparisons (Fig. 5). Visual discrimination analysis across sessions 1-4 was carried out after outlier elimination using the ROUT method with Q = 0.01%. All latency analyses were performed using mean session values per mouse.

DECLARATIONS

Funding

This study was funded by the Australian Research Council (ARC: DP120104117). CC and JN were supported by ARC Future Fellowships (FT110100292; FT140101327). MW was supported by an Australian Government Research Training Program Stipend.

Competing interests

The authors declare no competing interests or conflicts of interest.

Ethics approval and consent to participate

All animal breeding and animal experiments were performed with approval from the Monash Animal Research Platform animal ethics committee (Monash University, Clayton, Australia) and the Florey Institute of Neuroscience and Mental Health Animal Ethics Committee (Melbourne University, Parkville, Australia) in accordance with Australian National Health and Medical Research Guidelines on Ethics in Animal Experiments.

Consent to participate

Not applicable.

Consent for publication

Not applicable.

Availability of data and material

All data generated or analysed during this study are included in this published article and its supplementary information files.

Code availability

Not applicable.

Authors' contributions

MW, JN & CC designed experiments. MW, GW & JL performed experiments. MW, GW, JN & CC analysed data. MW wrote the manuscript. JN & CC supervised the study and edited the manuscript. All authors reviewed the manuscript.

REFERENCES

1. Gebert LFR, MacRae IJ. Regulation of microRNA function in animals. Nat Rev Mol Cell Biol. Nature Publishing Group; 2019;20:21–37.

2. Friedman RC, Farh KK, Burge CB, Bartel DP. Most mammalian mRNAs are conserved targets of microRNAs. Genome Res. 2009;19:92–105.

3. Jonas S, Izaurralde E. Towards a molecular understanding of microRNA-mediated gene silencing. Nat Rev Genet. Nature Publishing Group; 2015;16:421–33.

4. Guven-Ozkan T, Busto GU, Schutte SS, Cervantes-Sandoval I, O'Dowd DK, Davis RL. MiR-980 Is a Memory Suppressor MicroRNA that Regulates the Autism-Susceptibility Gene A2bp1. Cell Rep. 2016;14:1698–709.

5. Williams SM, An JY, Edson J, Watts M, Murigneux V, Whitehouse AJO, et al. An integrative analysis of non-coding regulatory DNA variations associated with autism spectrum disorder. Mol Psychiatry [Internet]. 2018/04/29 ed. 2018; Available from: https://www.ncbi.nlm.nih.gov/pubmed/29703944

6. Zampa F, Bicker S, Schratt G. Activity-Dependent Pre-miR-134 Dendritic Localization Is Required for Hippocampal Neuron Dendritogenesis. Front Mol Neurosci [Internet]. 2018;11. Available from: http://www.ncbi.nlm.nih.gov/pubmed/29942249

7. Banerjee S, Neveu P, Kosik KS. A coordinated local translational control point at the synapse involving relief from silencing and MOV10 degradation. Neuron. 2009;64:871–84.

8. Lugli G, Larson J, Demars MP, Smalheiser NR. Primary microRNA precursor transcripts are localized at post-synaptic densities in adult mouse forebrain. J Neurochem. 2012;123:459–66.

9. Smalheiser NR, Lugli G. microRNA regulation of synaptic plasticity. Neuromolecular Med. 2009/05/22 ed. 2009;11:133–40.

10. Chan SY, Zhang YY, Hemann C, Mahoney CE, Zweier JL, Loscalzo J. MicroRNA-210 controls mitochondrial metabolism during hypoxia by repressing the iron-sulfur cluster assembly proteins ISCU1/2. Cell Metab. 2009;10:273–84.

11. Crosby ME, Kulshreshtha R, Ivan M, Glazer PM. MicroRNA regulation of DNA repair gene expression in hypoxic stress. Cancer Res. 2009;69:1221–9.

12. Zhang Z, Sun H, Dai H, Walsh RM, Imakura M, Schelter J, et al. MicroRNA miR-210 modulates cellular response to hypoxia through the MYC antagonist MNT. Cell Cycle. 2009;8:2756–68.

13. Ren D, Yang Q, Dai Y, Guo W, Du H, Song L, et al. Oncogenic miR-210-3p promotes prostate cancer cell EMT and bone metastasis via NF-kappaB signaling pathway. Mol Cancer. 2017/07/12 ed. 2017;16:117.

14. Sun FB, Lin Y, Li SJ, Gao J, Han B, Zhang CS. MiR-210 knockdown promotes the development of pancreatic cancer via upregulating E2F3 expression. Eur Rev Med Pharmacol Sci. 2018/12/24 ed. 2018;22:8640–8.

15. Xie S, Liu G, Huang J, Hu HB, Jiang W. miR-210 promotes lung adenocarcinoma proliferation, migration, and invasion by targeting lysyl oxidase-like 4. J Cell Physiol [Internet]. 2019/01/12 ed. 2019; Available from: https://www.ncbi.nlm.nih.gov/pubmed/30633357

16. Yang X, Shi L, Yi C, Yang Y, Chang L, Song D. MiR-210-3p inhibits the tumor growth and metastasis of bladder cancer via targeting fibroblast growth factor receptor-like 1. Am J Cancer Res. 2017/09/02 ed. 2017;7:1738–53.

17. Fasanaro P, D'Alessandra Y, Di Stefano V, Melchionna R, Romani S, Pompilio G, et al. MicroRNA-210 modulates endothelial cell response to hypoxia and inhibits the receptor tyrosine kinase ligand Ephrin-A3. J Biol Chem. 2008;283:15878–83.

18. Pulkkinen K, Malm T, Turunen M, Koistinaho J, Yla-Herttuala S. Hypoxia induces microRNA miR-210 in vitro and in vivo ephrin-A3 and neuronal pentraxin 1 are potentially regulated by miR-210. FEBS Lett. 2008;582:2397–401.

19. Hu S, Huang M, Li Z, Jia F, Ghosh Z, Lijkwan MA, et al. MicroRNA-210 as a novel therapy for treatment of ischemic heart disease. Circulation. 2010;122:S124-31.

20. Ma Q, Dasgupta C, Li Y, Huang L, Zhang L. MicroRNA-210 Downregulates ISCU and Induces Mitochondrial Dysfunction and Neuronal Death in Neonatal Hypoxic-Ischemic Brain Injury. Mol Neurobiol [Internet]. 2019/01/19 ed. 2019; Available from: https://www.ncbi.nlm.nih.gov/pubmed/30656514

21. Cristino AS, Barchuk AR, Freitas FC, Narayanan RK, Biergans SD, Zhao Z, et al. Neuroligin-associated microRNA-932 targets actin and regulates memory in the honeybee. Nat Commun [Internet]. 2014;5. Available from: http://www.ncbi.nlm.nih.gov/pubmed/25409902

22. Behura SK, Whitfield CW. Correlated expression patterns of microRNA genes with age-dependent behavioural changes in honeybee. Insect Mol Biol. 2010;19:431–9.

23. Chen X, Rosbash M. MicroRNA-92a is a circadian modulator of neuronal excitability in Drosophila. Nat Commun. 2017/03/10 ed. 2017;8:14707.

24. Cusumano P, Biscontin A, Sandrelli F, Mazzotta GM, Tregnago C, De Pitta C, et al. Modulation of miR-210 alters phasing of circadian locomotor activity and impairs projections of PDF clock neurons in Drosophila melanogaster. PLoS Genet. 2018/07/17 ed. 2018;14:e1007500.

25. Zeng L, He X, Wang Y, Tang Y, Zheng C, Cai H, et al. MicroRNA-210 overexpression induces angiogenesis and neurogenesis in the normal adult mouse brain. Gene Ther. 2014;21:37–43.

26. Abdullah AI, Zhang H, Nie Y, Tang W, Sun T. CDK7 and miR-210 Co-regulate Cell-Cycle Progression of Neural Progenitors in the Developing Neocortex. Stem Cell Rep. 2016;7:69–79.

27. Wang J, Zhang Y, Xu F. Function and mechanism of microRNA-210 in acute cerebral infarction. Exp Ther Med. 2018/02/13 ed. 2018;15:1263–8.

28. Cogswell JP, Ward J, Taylor IA, Waters M, Shi Y, Cannon B, et al. Identification of miRNA changes in Alzheimer's disease brain and CSF yields putative biomarkers and insights into disease pathways. J Alzheimers Dis. 2008;14:27–41.

29. Hebert SS, Horre K, Nicolai L, Papadopoulou AS, Mandemakers W, Silahtaroglu AN, et al. Loss of microRNA cluster miR-29a/b-1 in sporadic Alzheimer's disease correlates with increased BACE1/beta-secretase expression. Proc Natl Acad Sci U A. 2008;105:6415–20.

30. Zhu Y, Li C, Sun A, Wang Y, Zhou S. Quantification of microRNA-210 in the cerebrospinal fluid and serum: Implications for Alzheimer's disease. Exp Ther Med. 2015;9:1013–7.

31. Gorter JA, Iyer A, White I, Colzi A, van Vliet EA, Sisodiya S, et al. Hippocampal subregion-specific microRNA expression during epileptogenesis in experimental temporal lobe epilepsy. Neurobiol Dis. 2014;62:508–20.

32. Kretschmann A, Danis B, Andonovic L, Abnaof K, van Rikxoort M, Siegel F, et al. Different microRNA profiles in chronic epilepsy versus acute seizure mouse models. J Mol Neurosci. 2015;55:466–79.

33. Schouten M, Fratantoni SA, Hubens CJ, Piersma SR, Pham TV, Bielefeld P, et al. MicroRNA-124 and -137 cooperativity controls caspase-3 activity through BCL2L13 in hippocampal neural stem cells. Sci Rep [Internet]. 2015;5. Available from: http://www.ncbi.nlm.nih.gov/pubmed/26207921

34. Ren Z, Yu J, Wu Z, Si W, Li X, Liu Y, et al. MicroRNA-210-5p Contributes to Cognitive Impairment in Early Vascular Dementia Rat Model Through Targeting Snap25. Front Mol Neurosci. 2018/11/30 ed. 2018;11:388.

35. Watts ME, Williams SM, Nithianantharajah J, Claudianos C. Hypoxia-Induced MicroRNA-210 Targets Neurodegenerative Pathways. Noncoding RNA [Internet]. 2018/04/17 ed. 2018;4. Available from: https://www.ncbi.nlm.nih.gov/pubmed/29657306

36. Pickard L, Noel J, Duckworth JK, Fitzjohn SM, Henley JM, Collingridge GL, et al. Transient synaptic activation of NMDA receptors leads to the insertion of native AMPA receptors at hippocampal neuronal plasma membranes. Neuropharmacology. 2001;41:700–13.

37. Jaafari N, Konopacki FA, Owen TF, Kantamneni S, Rubin P, Craig TJ, et al. SUMOylation is required for glycine-induced increases in AMPA receptor surface expression (ChemLTP) in hippocampal neurons. PLoS One [Internet]. 2013;8. Available from: http://www.ncbi.nlm.nih.gov/pubmed/23326329

38. Rimoldi S, Terova G, Ceccuzzi P, Marelli S, Antonini M, Saroglia M. HIF-1alpha mRNA levels in Eurasian perch (Perca fluviatilis) exposed to acute and chronic hypoxia. Mol Biol Rep. 2012;39:4009–15.

39. O'Sullivan NC, McGettigan PA, Sheridan GK, Pickering M, Conboy L, O'Connor JJ, et al. Temporal change in gene expression in the rat dentate gyrus following passive avoidance learning. J Neurochem. 2007/02/15 ed. 2007;101:1085–98.

40. Rampon C, Jiang CH, Dong H, Tang YP, Lockhart DJ, Schultz PG, et al. Effects of environmental enrichment on gene expression in the brain. Proc Natl Acad Sci U A. 2000/11/09 ed. 2000;97:12880–4.

41. Ryan MM, Mason-Parker SE, Tate WP, Abraham WC, Williams JM. Rapidly induced gene networks following induction of long-term potentiation at perforant path synapses in vivo. Hippocampus. 2011;21:541–53.

42. Ryan MM, Ryan B, Kyrke-Smith M, Logan B, Tate WP, Abraham WC, et al. Temporal profiling of gene networks associated with the late phase of long-term potentiation in vivo. PLoS One [Internet]. 2012;7. Available from: http://www.ncbi.nlm.nih.gov/pubmed/22802965

43. Park CY, Jeker LT, Carver-Moore K, Oh A, Liu HJ, Cameron R, et al. A resource for the conditional ablation of microRNAs in the mouse. Cell Rep. 2012;1:385–91.

44. Hale A, Lee C, Annis S, Min PK, Pande R, Creager MA, et al. An Argonaute 2 Switch Regulates Circulating miR-210 to Coordinate Hypoxic Adaptation across Cells. Biochim Biophys Acta [Internet]. 2014/07/02 ed. 2014; Available from: http://www.ncbi.nlm.nih.gov/pubmed/24983771

45. Nithianantharajah J, Grant SG. Cognitive components in mice and humans: combining genetics and touchscreens for medical translation. Neurobiol Learn Mem. 2013;105:13–9.

46. Horner AE, Heath CJ, Hvoslef-Eide M, Kent BA, Kim CH, Nilsson SR, et al. The touchscreen operant platform for testing learning and memory in rats and mice. Nat Protoc. 2013;8:1961–84.

47. Mar AC, Horner AE, Nilsson SR, Alsio J, Kent BA, Kim CH, et al. The touchscreen operant platform for assessing executive function in rats and mice. Nat Protoc. 2013;8:1985–2005.

48. Oomen CA, Hvoslef-Eide M, Heath CJ, Mar AC, Horner AE, Bussey TJ, et al. The touchscreen operant platform for testing working memory and pattern separation in rats and mice. Nat Protoc. 2013;8:2006–21.

49. Nithianantharajah J, McKechanie AG, Stewart TJ, Johnstone M, Blackwood DH, St Clair D, et al. Bridging the translational divide: identical cognitive touchscreen testing in mice and humans carrying mutations in a disease-relevant homologous gene. Sci Rep. 2015/10/02 ed. 2015;5:14613.

50. Ryan TJ, Kopanitsa MV, Indersmitten T, Nithianantharajah J, Afinowi NO, Pettit C, et al. Evolution of GluN2A/B cytoplasmic domains diversified vertebrate synaptic plasticity and behavior. Nat Neurosci. 2013;16:25–32.

51. Nithianantharajah J, Komiyama NH, McKechanie A, Johnstone M, Blackwood DH, St Clair D, et al. Synaptic scaffold evolution generated components of vertebrate cognitive complexity. Nat Neurosci. 2013;16:16–24.

52. Bussey TJ, Padain TL, Skillings EA, Winters BD, Morton AJ, Saksida LM. The touchscreen cognitive testing method for rodents: how to get the best out of your rat. Learn Mem. 2008;15:516–23.

53. Adamcio B, Sperling S, Hagemeyer N, Walkinshaw G, Ehrenreich H. Hypoxia inducible factor stabilization leads to lasting improvement of hippocampal memory in healthy mice. Behav Brain Res. 2010;208:80–4.

54. Tomita S, Ueno M, Sakamoto M, Kitahama Y, Ueki M, Maekawa N, et al. Defective brain development in mice lacking the Hif-1alpha gene in neural cells. Mol Cell Biol. 2003;23:6739–49.

55. Watts ME, Pocock R, Claudianos C. Brain Energy and Oxygen Metabolism: Emerging Role in Normal Function and Disease. Front Mol Neurosci. 2018/07/11 ed. 2018;11:216.

56. Hu YW, Jiang JJ, Yan G, Wang RY, Tu GJ. MicroRNA-210 promotes sensory axon regeneration of adult mice in vivo and in vitro. Neurosci Lett. 2016;622:61–6.

57. Cang J, Kaneko M, Yamada J, Woods G, Stryker MP, Feldheim DA. Ephrin-as guide the formation of functional maps in the visual cortex. Neuron. 2005;48:577–89.

58. Murai KK, Nguyen LN, Irie F, Yamaguchi Y, Pasquale EB. Control of hippocampal dendritic spine morphology through ephrin-A3/EphA4 signaling. Nat Neurosci. 2003;6:153–60.

59. Du H, Guo L, Yan S, Sosunov AA, McKhann GM, Yan SS. Early deficits in synaptic mitochondria in an Alzheimer's disease mouse model. Proc Natl Acad Sci U A. 2010;107:18670–5.

60. Wirths O, Multhaup G, Czech C, Blanchard V, Moussaoui S, Tremp G, et al. Intraneuronal Abeta accumulation precedes plaque formation in beta-amyloid precursor protein and presenilin-1 double-transgenic mice. Neurosci Lett. 2001;306:116–20.

61. Liu Y, Liu F, Iqbal K, Grundke-Iqbal I, Gong CX. Decreased glucose transporters correlate to abnormal hyperphosphorylation of tau in Alzheimer disease. FEBS Lett. 2008;582:359–64.

62. Rohrbach S, Simm A, Pregla R, Franke C, Katschinski DM. Age-dependent increase of prolyl-4-hydroxylase domain (PHD) 3 expression in human and mouse heart. Biogerontology. 2005;6:165–71.

63. Chang EI, Loh SA, Ceradini DJ, Chang EI, Lin SE, Bastidas N, et al. Age decreases endothelial progenitor cell recruitment through decreases in hypoxia-inducible factor 1alpha stabilization during ischemia. Circulation. 2007;116:2818–29.

64. Niecknig H, Tug S, Reyes BD, Kirsch M, Fandrey J, Berchner-Pfannschmidt U. Role of reactive oxygen species in the regulation of HIF-1 by prolyl hydroxylase 2 under mild hypoxia. Free Radic Res. 2012;46:705–17.

65. Ward CP, McCoy JG, McKenna JT, Connolly NP, McCarley RW, Strecker RE. Spatial learning and memory deficits following exposure to 24 h of sleep fragmentation or intermittent hypoxia in a rat model of obstructive sleep apnea. Brain Res. 2009;1294:128–37.

66. Row BW, Liu R, Xu W, Kheirandish L, Gozal D. Intermittent hypoxia is associated with oxidative stress and spatial learning deficits in the rat. Am J Respir Crit Care Med. 2003;167:1548–53.

67. Rybnikova E, Vataeva L, Tyulkova E, Gluschenko T, Otellin V, Pelto-Huikko M, et al. Mild hypoxia preconditioning prevents impairment of passive avoidance learning and suppression of brain NGFI-A expression induced by severe hypoxia. Behav Brain Res. 2005;160:107–14.

68. Jones NM, Bergeron M. Hypoxic Preconditioning Induces Changes in HIF-1 Target Genes in Neonatal Rat Brain. J Cereb Blood Flow Metab. SAGE Publications Ltd STM; 2001;21:1105–14.

69. Sun MK, Xu H, Alkon DL. Pharmacological protection of synaptic function, spatial learning, and memory from transient hypoxia in rats. J Pharmacol Exp Ther. 2002/01/24 ed. 2002;300:408–16.

70. Katchanov J, Waeber C, Gertz K, Gietz A, Winter B, Bruck W, et al. Selective neuronal vulnerability following mild focal brain ischemia in the mouse. Brain Pathol. 2003;13:452–64.

71. Frahm C, Haupt C, Witte OW. GABA neurons survive focal ischemic injury. Neuroscience. 2004;127:341–6.

72. Ramamoorthy P, Shi H. Ischemia induces different levels of hypoxia inducible factor-1alpha protein expression in interneurons and pyramidal neurons. Acta Neuropathol Commun [Internet]. 2014;2. Available from: http://www.ncbi.nlm.nih.gov/pubmed/24887017

73. Gruber AJ, Calhoon GG, Shusterman I, Schoenbaum G, Roesch MR, O'Donnell P. More is less: a disinhibited prefrontal cortex impairs cognitive flexibility. J Neurosci. 2010;30:17102–10.

74. Korotkova T, Fuchs EC, Ponomarenko A, von Engelhardt J, Monyer H. NMDA receptor ablation on parvalbumin-positive interneurons impairs hippocampal synchrony, spatial representations, and working memory. Neuron. 2010;68:557–69.

75. Murray AJ, Sauer JF, Riedel G, McClure C, Ansel L, Cheyne L, et al. Parvalbumin-positive CA1 interneurons are required for spatial working but not for reference memory. Nat Neurosci. 2011;14:297–9.

76. Sohal VS, Zhang F, Yizhar O, Deisseroth K. Parvalbumin neurons and gamma rhythms enhance cortical circuit performance. Nature. 2009;459:698–702.

77. Fuller RL, Luck SJ, Braun EL, Robinson BM, McMahon RP, Gold JM. Impaired control of visual attention in schizophrenia. J Abnorm Psychol. 2006;115:266–75.

78. Holt DJ, Lebron-Milad K, Milad MR, Rauch SL, Pitman RK, Orr SP, et al. Extinction memory is impaired in schizophrenia. Biol Psychiatry. 2009;65:455–63.

79. Waltz JA, Gold JM. Probabilistic reversal learning impairments in schizophrenia: further evidence of orbitofrontal dysfunction. Schizophr Res. 2007;93:296–303.

80. Zhang ZJ, Reynolds GP. A selective decrease in the relative density of parvalbumin-immunoreactive neurons in the hippocampus in schizophrenia. Schizophr Res. 2002;55:1–10.

81. Gittis AH, Leventhal DK, Fensterheim BA, Pettibone JR, Berke JD, Kreitzer AC. Selective inhibition of striatal fast-spiking interneurons causes dyskinesias. J Neurosci. 2011;31:15727–31.

82. Mallet N, Ballion B, Le Moine C, Gonon F. Cortical inputs and GABA interneurons imbalance projection neurons in the striatum of parkinsonian rats. J Neurosci. 2006;26:3875–84.

83. Verret L, Mann EO, Hang GB, Barth AM, Cobos I, Ho K, et al. Inhibitory interneuron deficit links altered network activity and cognitive dysfunction in Alzheimer model. Cell. 2012;149:708–21.

84. Xu M, Kobets A, Du JC, Lennington J, Li L, Banasr M, et al. Targeted ablation of cholinergic interneurons in the dorsolateral striatum produces behavioral manifestations of Tourette syndrome. Proc Natl Acad Sci U A. 2015;112:893–8.

85. Dinocourt C, Petanjek Z, Freund TF, Ben-Ari Y, Esclapez M. Loss of interneurons innervating pyramidal cell dendrites and axon initial segments in the CA1 region of the hippocampus following pilocarpine-induced seizures. J Comp Neurol. 2003;459:407–25.

86. Sayin U, Osting S, Hagen J, Rutecki P, Sutula T. Spontaneous seizures and loss of axo-axonic and axo-somatic inhibition induced by repeated brief seizures in kindled rats. J Neurosci. 2003;23:2759–68.

87. Chen C, Ridzon DA, Broomer AJ, Zhou Z, Lee DH, Nguyen JT, et al. Real-time quantification of microRNAs by stem-loop RT-PCR. Nucleic Acids Res [Internet]. 2005;33. Available from: http://www.ncbi.nlm.nih.gov/pubmed/16314309

88. Kramer MF. Stem-loop RT-qPCR for miRNAs. Curr Protoc Mol Biol [Internet]. 2011;Chapter 15. Available from: http://www.ncbi.nlm.nih.gov/pubmed/21732315

89. Varkonyi-Gasic E, Wu R, Wood M, Walton EF, Hellens RP. Protocol: a highly sensitive RT-PCR method for detection and quantification of microRNAs. Plant Methods [Internet]. 2007;3. Available from: http://www.ncbi.nlm.nih.gov/pubmed/17931426

FIGURE LEDGENDS

Figure 1: Neuronal miR-210 expression *in vitro*. Localisation and activity induction of miR-210 were analysed in primary hippocampal neurons cultured from wild-type C57BL/6 mice. **a-f.** Fluorescent In-Situ Hybridisation (FISH) was used to detect miR-210 in fixed neurons at DIV-21. **a-c.** miR-210 LNA was detected throughout the cell body and within dendritic processes and synaptic structures. **d-f.** No signal was detected in neurons stained with negative control Scramble-miR LNA probe. Green fluorescence = fluorescein, blue = DAPI, magenta = dendritic marker, MAP2. Scale bar = 30 μm a-f, 12.8 μm inset. **g-i.** Activity induction of mature miR-210 was quantified by qRT-PCR **g.** Relative expression of miR-210 24 h after K^+ activation, *n* = 9, two sample t-test. **h.** Relative expression of miR-210 24 h after glycine-induced Chem-LTP, *n* = 6, two sample t-test. **i.** Relative expression of *Hif-1α* and *Hif-2α* at 20 min, 5 hr, 12 hr and 24 h following *in vitro* K^+ activation, *n* = 3, two-sample t-test. Data represent mean values, error bars represent SEM, ** p <0.01. Expression data was normalised to either *Rn5s* (miR-210) or *Tbp* and *Hprt1* (protein-coding genes).

Figure 2: Effect of miR-210 knockout on neuronal metabolic function. Levels of cellular ROS and mitochondrial membrane potential were measured in live hippocampal neurons cultured from miR-210 KO and littermate tg CTRL neurons using DCFDA and TMRE fluorescent indicators, respectively, following 48 h incubation in 1% O_2. **a-b.** Representative images of TMRE staining in miR-210 KO and tg CTRL cultures. **c.** Quantification of TMRE fluorescence mean intensity within the cell soma, *n* = 41 (tg CTRL), 54 (miR-210 KO). **d-e.** Representative images of DCFDA staining in miR-210 KO and tg CTRL cultures **f.** Quantification of DCFDA fluorescence mean intensity within the cell soma, *n* = 38 (tg CTRL), *n* = 88 (miR-210 KO). Data represent mean values, error bars represent SEM, *** p <0.001, two sample t-test. Scale bar = 25 μm in all images.

Figure 3: Dendritic morphology in miR-210 knockout hippocampal neurons. Scholl analysis of dendritic arbours was performed on miR-210 KO and littermate tg CTRL neurons *in vitro*, using MAP2 as a dendritic marker. **a,b**. Representative single-channel images of MAP2 staining in miR-210 KO and tg CTRL neurons used for analysis. **c.** Average Scholl curve of neurons, plotted as mean number of intersections per radius. **d.** Total number of intersections per neuron. **e.** Average size of the dendritic arbour. **f.** Average branching measured as Ramification index. Data represent mean values, error bars represent SEM, *n* = 184, Kolmogorov-Smirnov test, ** p <0.01, *** p <0.001. Scale bar = 50 μm.

Figure 4: Touchscreen cognitive testing of miR-210 knockout mice in the visual discrimination task. a. Schematic of the touchscreen testing set-up for pre-training where a single visual stimulus is presented in a pseudo-randomised location. **b.** Number of sessions taken for mice

to reach criterion on each pre-training stage. All mice rapidly completed pre-training in the minimum number of sessions. **c**. Schematic of the visual discrimination touchscreen task, a rewarded (CS+) and an unrewarded (CS-) stimuli are presented simultaneously (location pseudorandomised for each trial). **d.** Stimuli used for visual discrimination and reversal learning tasks. **e-g.** Primary measures of performance on the visual discrimination task. **e.** Total number of trials taken to reach visual discrimination learning criterion. **f.** Total number of errors (incorrect responses) to reach visual discrimination learning criterion. **g.** Total number of correction trials to reach visual discrimination learning criterion. Data represent mean values, error bars represent SEM, *n* = 6 (tg CTRL), *n* = 7 (miR-210 KO), two-sample t-test.

Figure 5: Reversal learning in miR-210 knockout mice. a. In the reversal learning touchscreen task, the previously allocated CS+ and CS- were switched. **b-i.** Analysis of reversal learning across sessions. **b.** Accuracy (percentage of correct responses). **c.** Perseverative Index (correction trials/incorrect responses). **d.** Time taken to complete sessions. **e.** Latency to initiate trials (following correct and incorrect responses) after the inter-trial interval**. f.** Latency to initiate trials following correct responses. **g.** Latency to initiate trials following incorrect responses. **h.** Correct response latency (time taken to select CS+). **i.** Reward collection latency following correct responses. Legend for tg CTRL and miR-210 KO in **b** applies to all graphs. All latency analyses were performed using mean session values per mouse. Data represent group mean values, error lines represent SEM, *n* = 6 (tg CTRL), *n* = 7 (miR-210 KO), two-way repeated measures ANOVA or mixed effects model analysis with post hoc multiple comparison tests. * = significant effect of genotype (* $p < 0.05$, ** $p < 0.01$, *** $p < 0.001$), $ = significant genotype x session interaction ($$ $p < 0.01$, $$$ $p < 0.001$), # = significant post hoc multiple comparisons (# = $p < 0.05$).

Figure 6: Summary schematic of miR-210 in neuronal function. Using a miRNA:mRNA pull-down approach we previously identified miR-210 targeting pathways in human neuronal cells including oxidative phosphorylation genes associated with neurodegenerative diseases as well as several genes associated with neuronal and synaptic plasticity. Here we show that in primary mouse hippocampal neurons, miR-210 is expressed through out neurons including dendritic spines and increased by neuronal activity induced by K^+ and glycine. Loss of miR-210 in primary hippocampal neurons leads to functional effects related to known miR-210 targeting included altered metabolism and dendritic arbour morphology. *In vivo* miR-210 neuronal knockout mice display enhanced behavioral flexibility and drive to continue engaging in responding especially when contingencies in the environment change and updating of information is required, which may be supported by the observed molecular and cellular changes.

Figure 1

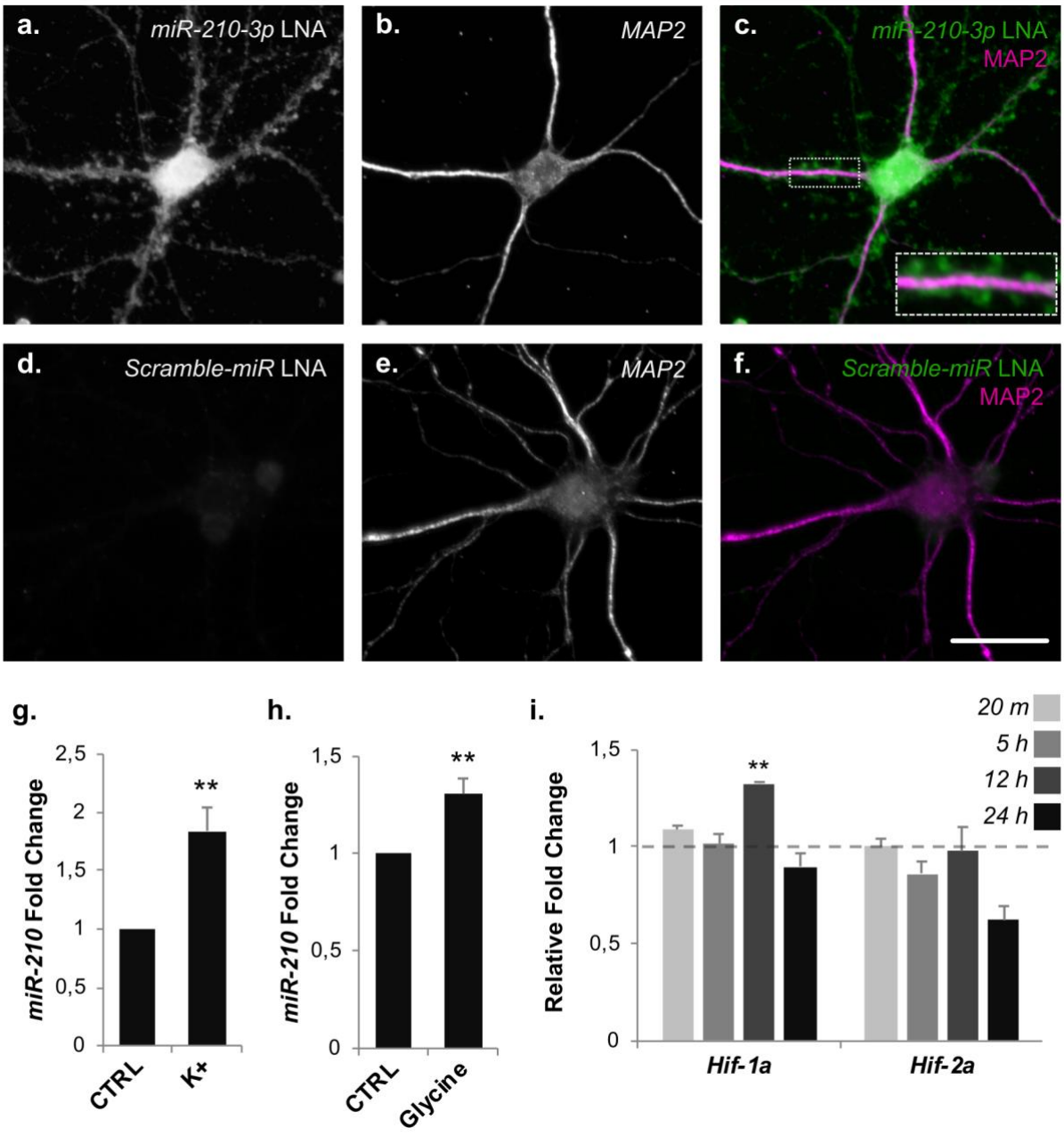
a.
miR-210-3p LNA
b.
MAP2
c.
miR-210-3p LNA
MAP2
d.
Scramble-miR LNA
e.
MAP2
f.
Scramble-miR LNA
MAP2
g.
miR-210 Fold Change
2,5
2
1,5
1
0,5
0
**
CTRL
K+
h.
miR-210 Fold Change
1,5
1
0,5
0
**
CTRL
Glycine
i.
Relative Fold Change
1,5
1
0,5
0
**
20 m
5 h
12 h
24 h
Hif-1a
Hif-2a

Figure 2

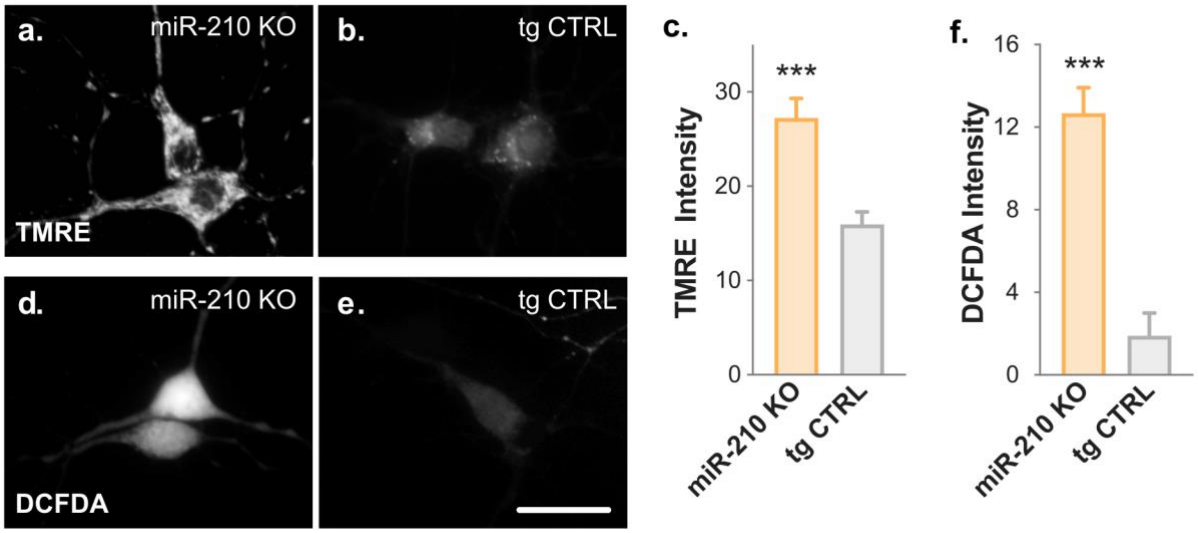
a.
miR-210 KO
b.
tg CTRL
TMRE
d.
miR-210 KO
e.
tg CTRL
DCFDA
c.
TMRE Intensity
***
30
20
10
0
miR-210 KO
tg CTRL
f.
DCFDA Intensity
***
16
12
8
4
0
miR-210 KO
tg CTRL

Figure 3

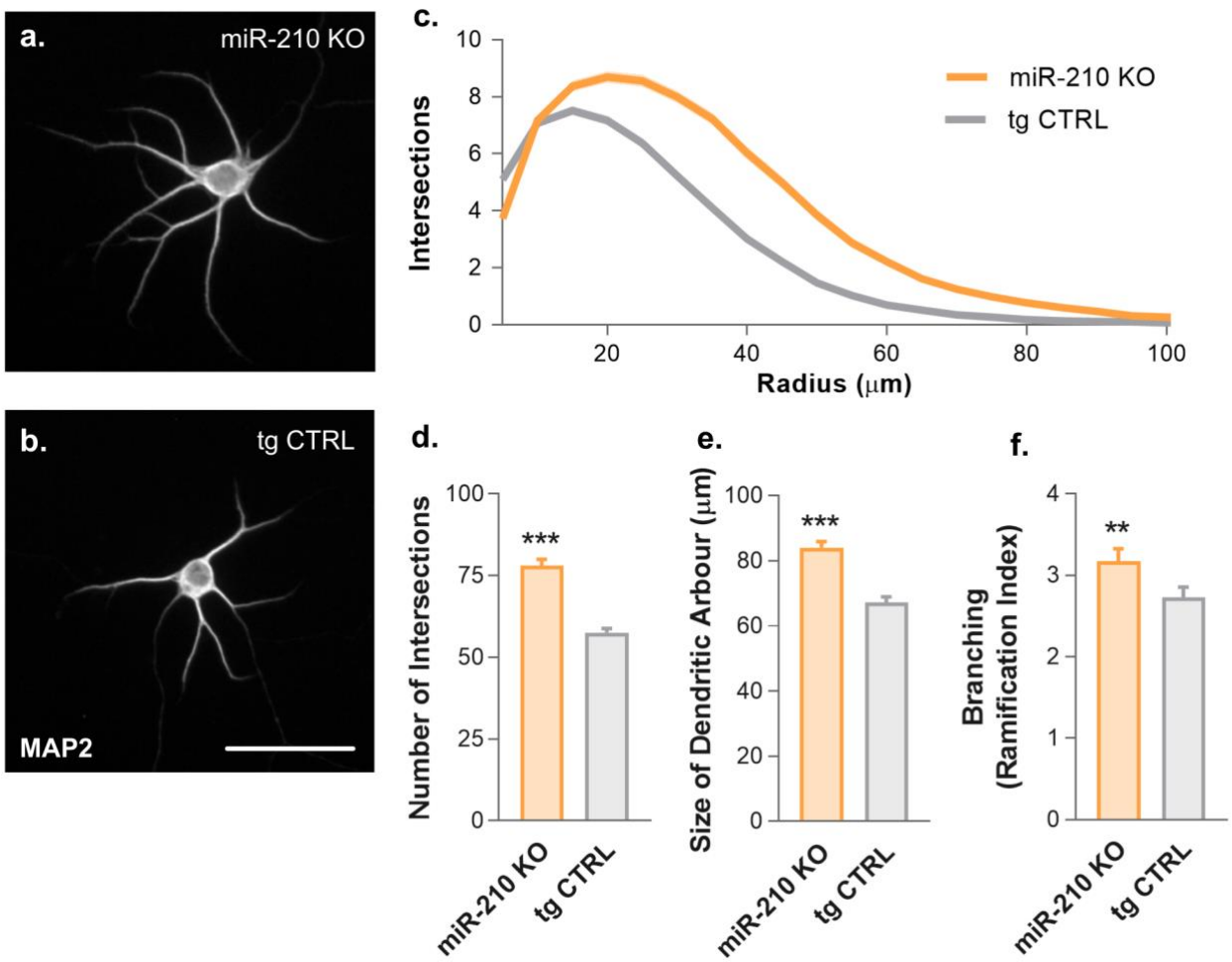
a.
miR-210 KO
b.
tg CTRL
MAP2
c.
Intersections
Radius (μm)
miR-210 KO
tg CTRL
d.
Number of Intersections
***
e.
Size of Dendritic Arbour (μm)
***
f.
Branching (Ramification Index)
**
miR-210 KO
tg CTRL

Figure 4

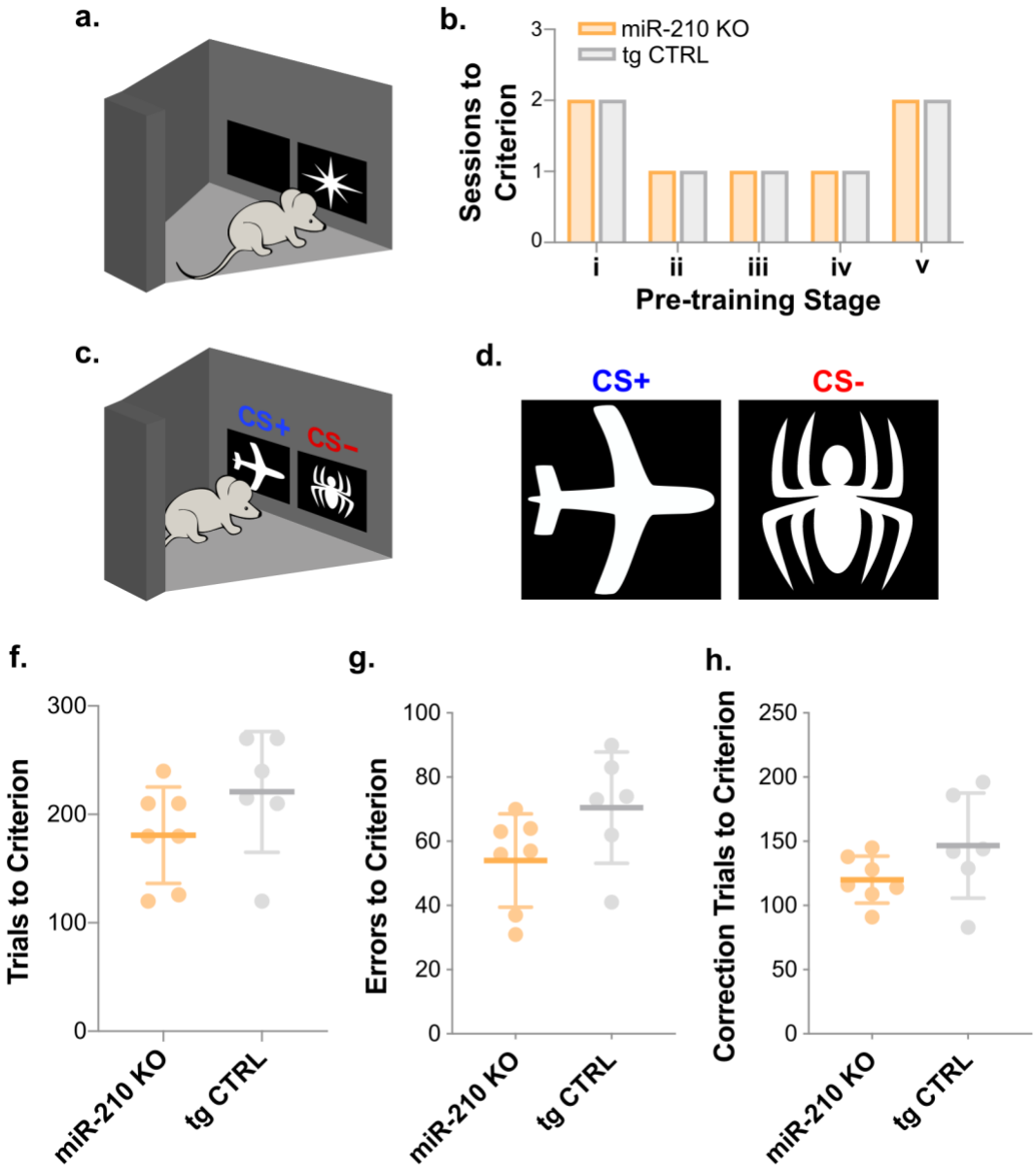
a.
b.
miR-210 KO
tg CTRL
Sessions to Criterion
3
2
1
0
i
ii
iii
iv
v
Pre-training Stage
c.
CS+
CS–
d.
CS+
CS-
f.
Trials to Criterion
300
200
100
0
miR-210 KO
tg CTRL
g.
Errors to Criterion
100
80
60
40
20
0
miR-210 KO
tg CTRL
h.
Correction Trials to Criterion
250
200
150
100
50
0
miR-210 KO
tg CTRL

Figure 5

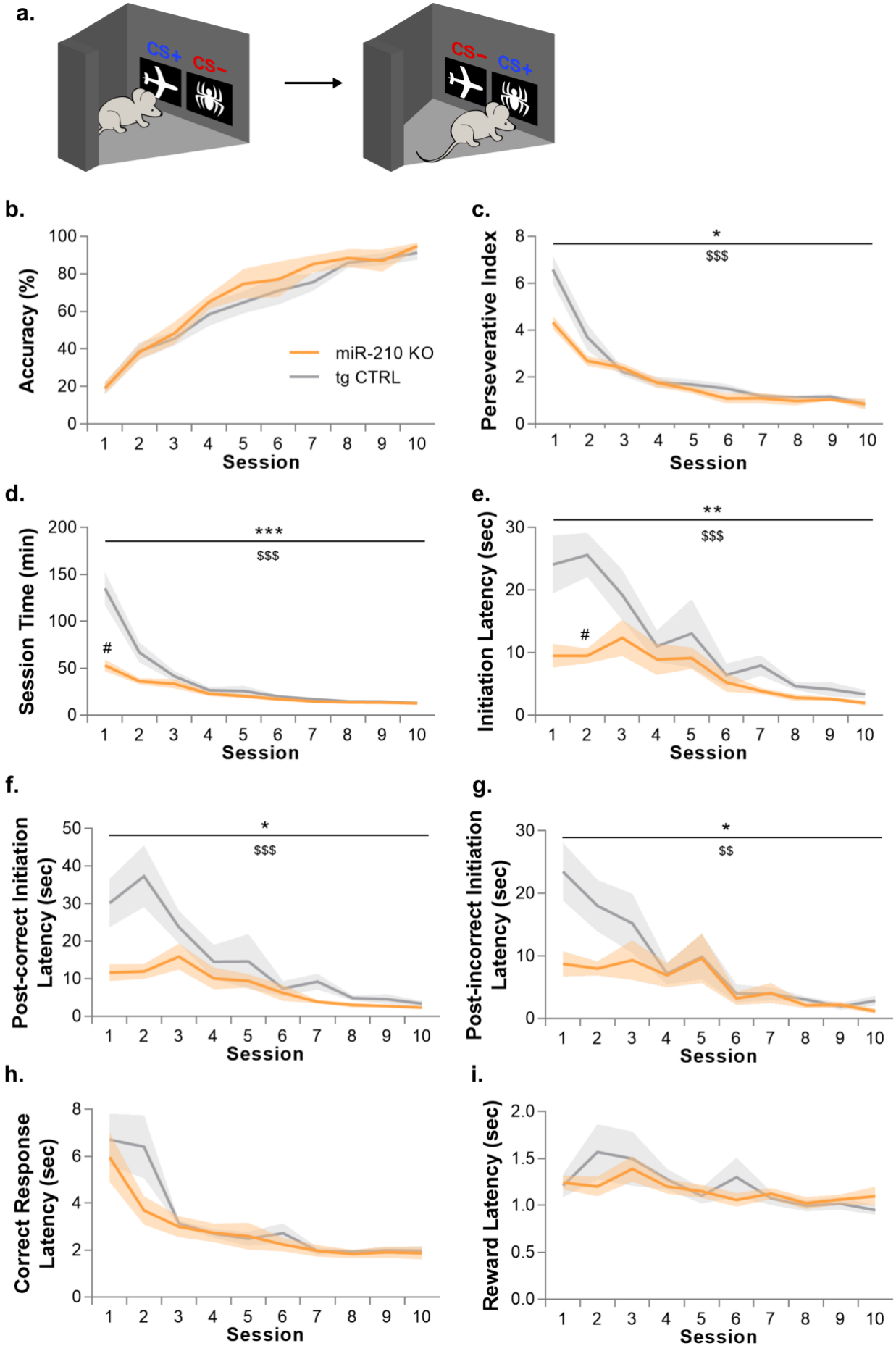
a.
CS+
CS−
CS−
CS+
b.
Accuracy (%)
Session
miR-210 KO
tg CTRL
c.
Perseverative Index
*
$$$
Session
d.
Session Time (min)
***
$$$
#
Session
e.
Initiation Latency (sec)
**
$$$
#
Session
f.
Post-correct Initiation Latency (sec)
*
$$$
Session
g.
Post-incorrect Initiation Latency (sec)
*
$$
Session
h.
Correct Response Latency (sec)
Session
i.
Reward Latency (sec)
Session

Figure 6

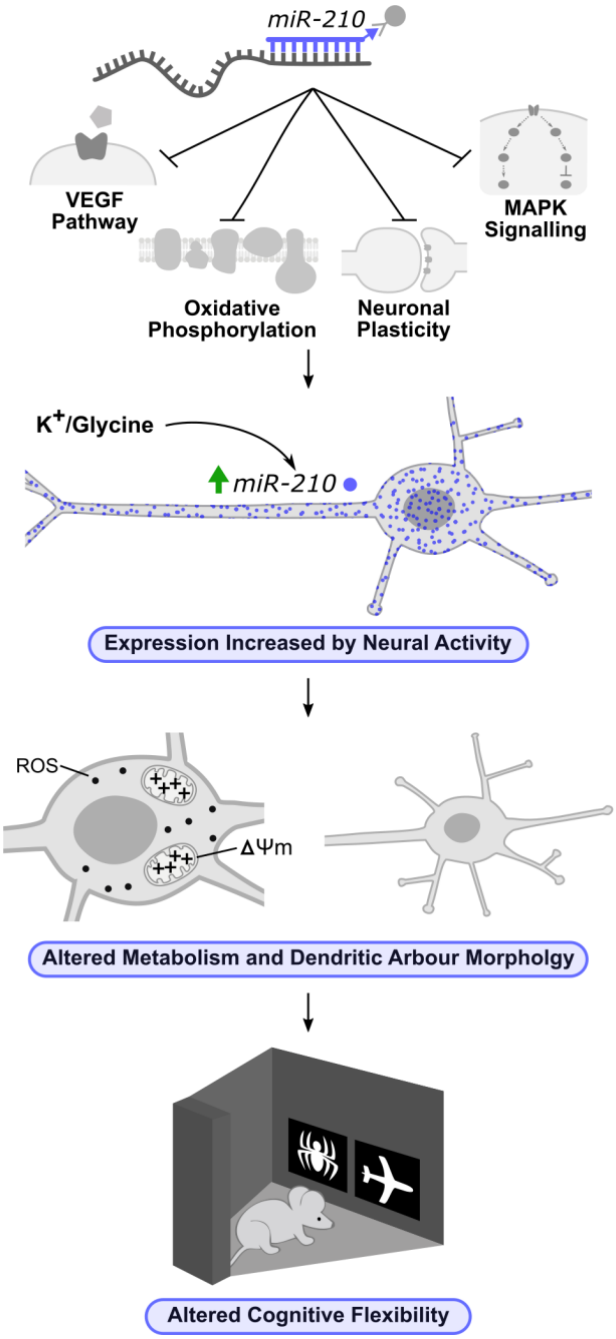
miR-210
VEGF Pathway
MAPK Signalling
Oxidative Phosphorylation
Neuronal Plasticity
K+/Glycine
miR-210
Expression Increased by Neural Activity
ROS
ΔΨm
Altered Metabolism and Dendritic Arbour Morpholgy
Altered Cognitive Flexibility

SUPPLEMENTARY INFORMATION

MicroRNA-210 Regulates Dendritic Morphology and Behavioural Flexibility in Mice

Michelle Watts[1], Gabrielle Williams[2], Jing Lu[3], Jess Nithianantharajah[4,5]*, Charles Claudianos[6,7]*

[1]Queensland Brain Institute, The University of Queensland, Brisbane, QLD, 4072, Australia. michelle.watts@ki.se
[2]School of Psychological Sciences, Monash University, Melbourne, VIC, 3800, Australia. gabbywilliams@gmail.com
[3]School of Psychological Sciences, Monash University, Melbourne, VIC, 3800, Australia. jing.lu2@monash.edu
[4]The Florey Institute of Neuroscience & Mental Health, Melbourne, VIC, 3052, Australia.
[5]Florey Department of Neuroscience, University of Melbourne, Melbourne, VIC, 3010, Australia. jess.n@florey.edu.au
[6]Queensland Brain Institute, The University of Queensland, Brisbane, QLD, 4072, Australia.
[7]Centre for Mental Health Research, The Australian National University, Canberra, ACT, 0200, Australia. charles.claudianos@anu.edu.au

*These authors contributed equally.

Correspondence should be addressed to:
J.N. (jess.n@florey.edu.au) or C.C. (charles.claudianos@anu.edu.au)

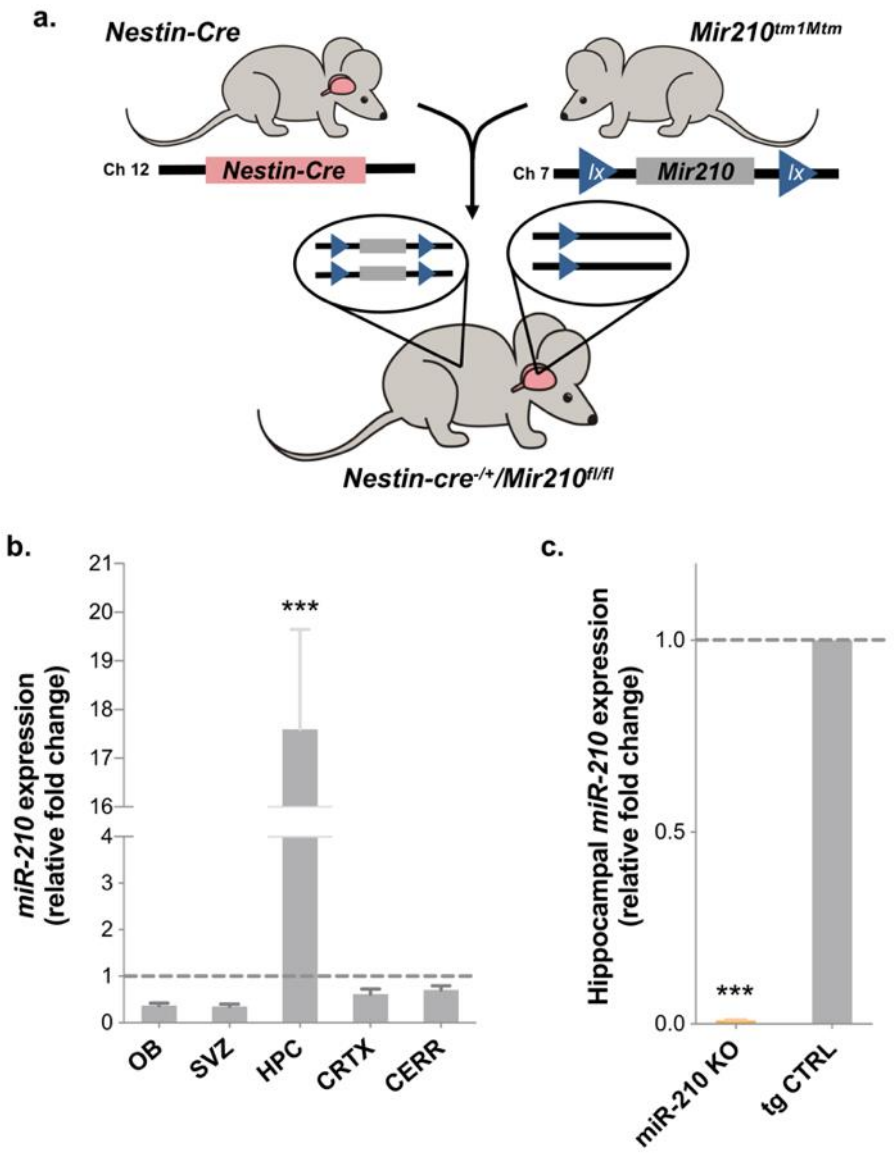

Supplementary Figure 1: Generation of miR-210 conditional neuronal knockout (KO) mice and quantification of miR-210 expression. a. Schematic of breeding to generate miR-210 KO mice. Heterozygous mice carrying a targeted miR-210 mutation with loxP sites flanking the miRNA stem-loop region were inbred to generate mice homozygous for the floxed allele (*miR-210*$^{loxP/loxP}$). *miR-210*$^{loxP/lox}$ mice were crossed with Nestin-Cre mice to generate mice homozygous for the floxed allele and heterozygous for Nestin-Cre (*miR-210*$^{-/-}$*;Nes-Cre*). **b.** miR-210 expression in control mice (*miR-210*$^{loxP/loxP}$) was quantified within various brain regions by qRT-PCR relative to average expression across all brain regions. OB = olfactory bulb, SVZ = sub-ventricular zone, HPC = hippocampus, CRTX = cortex, CERR = cerebellum, *n* = 4, pairwise t-test, adjusted. **c.** To confirm absence of miR-210 in KO mice, expression of miR-210 in the hippocampus of KO mice was quantified relative to hippocampal expression in control mice, *n* = 4 (tg CTRL), *n* = 3 (miR-210 KO), two-sample t-test. miR-210 was normalised to *Rnu6.* Data represent mean values, error bars represent SEM, *** = p<0.001.

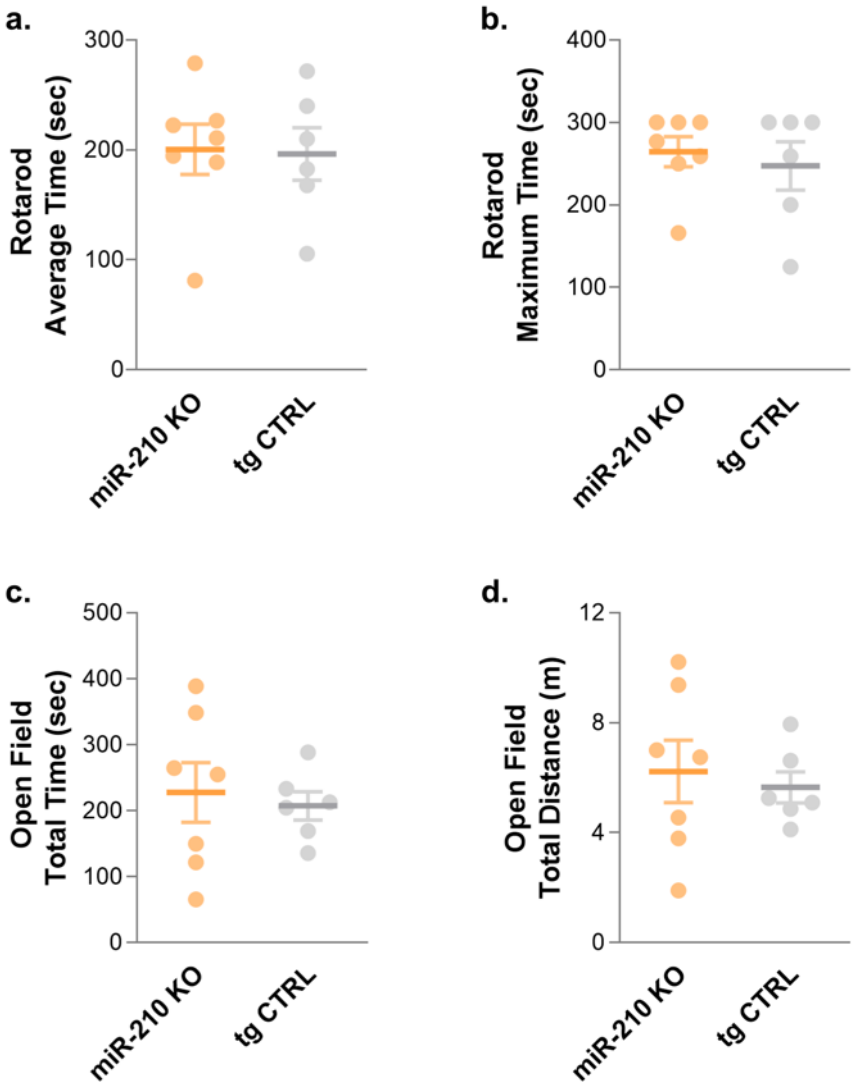

Supplementary Figure 2: Locomotor function and exploratory activity in miR-210 neuronal knockout (KO) mice. a. Time spent on accelerating rotarod (average over three trials). **b.** Maximum time spent on accelerating rotarod. **c.** Total ambulatory time in an open field chamber. **d.** Total distance travelled in an open field chamber. *n* = 6 (tg CTRL), *n* = 7 (miR-210 KO), two-sample t-test. Data represent mean values, error bars represent SEM.

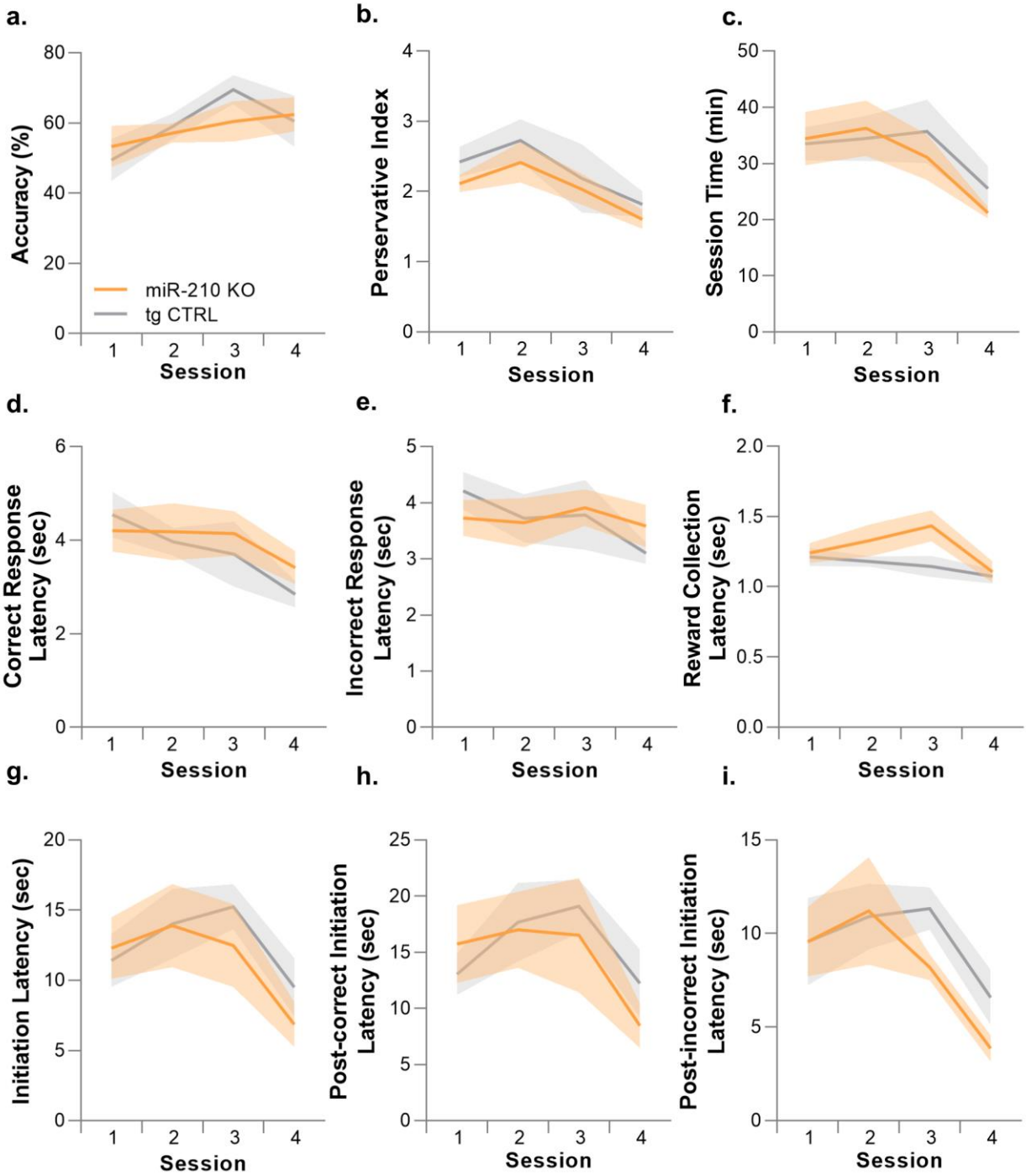

Supplementary Figure 3: Visual discrimination touchscreen task performance across the first four sessions. **a.** Accuracy (percentage of correct responses). **b.** Perservative Index (correction trials/incorrect responses). **c.** Time taken to complete sessions. **d.** Correct response latency **e.** Incorrect response latency. **f.** Reward collection latency following correct responses. **g.** Latency to initiate trials (following correct and incorrect responses) after the inter-trial interval. **h.** Latency to initiate trials following correct responses. **i.** Latency to initiate trials following incorrect responses. Legend in **a** applies to all graphs. Data represent mean values, error bars represent SEM, *n* = 6 (tg CTRL), *n* = 7 (miR-210 KO), two-way repeated measures ANOVA or mixed effects model analysis.

Target	*Primer: Sequence 5'>3'*	*Tm (°C)*
Rn5s	F: TCTCGTCTGATCTCGGAAGC	59.0
	RT/R: AGCCTACAGCACCCGGTATT	61.0
Rnu6	F: AACGCTTCACGAATTTGCGTG	60.9
	RT/R: GCTCGCTTCGGCAGCACA	63.7
miR-210	RT: GTCGTATCCAGTGCAGGGTCCGAGG TATTCGCACTGGATACGACTCAGCC	68.5
	F: GCCACTGTGCGTGTGACAGC	57.9
	R: CCAGTGCAGGGTCCGAGGTA	57.9
Hif-1α	F: ACCTTCATCGGAAACTCCAAAG	58.6
	R: CTGTTAGGCTGGGAAAAGTTAGG	60.0
Hif-2 α	F: CTGAGGAAGGAGAAATCCCGT	59.0
	R: TGTGTCCGAAGGAAGCTGATG	60.0
Hprt1	F: GAGGAGTCCTGTTGATGTTGCCAG	63.4
	R: GGCTGGCCTATAGGCTCATAGTGC	64.8
Tbp	F: AGAACAATCCAGACTAGCAGCA	59.4
	R: GGGAACTTCACATCACAGCTC	59.0

Supplementary Table 1: Primer sequences for qRT-PCR and cDNA synthesis. Sequences in black text are gene specific regions, blue text indicates stem-loop primer sequences, red text indicates additional non-specific bp's added to miR-210 forward qRT-PCR primer. F = forward, R = reverse, RT = reverse transcription.